Case Studies in Thermal Engineering 32 (2022) 101869

Contents lists available at ScienceDirect

Case Studies in Thermal Engineering

journal homepage: www.elsevier.com/locate/csite

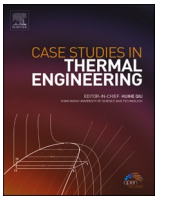

Experimental study on the thermal control of a roof-top collective building antenna using a porous matrix filled with Water-Copper nanofluid

F. Sastre [a], A. Martin-Garin [b], E. Martin [c,*], A. Velazquez [a], A. Baïri [d]

[a] Universidad Politécnica de Madrid, Fluid Mechanics and Aerospace Propulsion Department., Plaza del Cardenal Cisneros 3, 28040, Madrid, Spain
[b] Universidad del País Vasco, UPV/EHU, ENEDI Research Group, Department of Thermal Engineering, Plaza Europa 1, 20018, Donostia-San Sebastián, Spain
[c] Universidade de Vigo, Departamento de Ingeniería Mecánica, Máquinas y Motores Térmicos y Fluidos, Escuela de Ingeniería Industrial, Campus Marcosende, 36310, Vigo, Spain
[d] Université de Paris, Laboratoire Thermique Interfaces Environnement (LTIE), EA 4415, 50 rue de Sèvres, F-92410, Paris, France

HIGHLIGHTS

- Thermal control of a collective building finned cylindrical antenna.
- Nanofluid combined with porous media.
- Antenna temperature correlation for a range of governing parameters.
- Application case to a smart building collective antenna.

ARTICLE INFO

Keywords:
Smart building
Thermal regulation
Electronics engineering
Collective automation antenna
Nanofluid
Porous media

ABSTRACT

This experimental work addressed the thermal control a roof-top collective building antenna meant to control home equipment in smart buildings. The antenna was placed inside a concentric quasi-cylindrical cavity maintained at low temperature. Cooling was provided by a Water-Copper nanofluid saturated porous matrix placed between the antenna and the enclosure. The ratio of the thermal conductivity of the porous material to that of the water varied from 4 up to 41.2. The nanoparticles volume fraction varied between 0% and 5%. The main result was a new semi-empirical correlation that allows for the determination of the antenna's average surface temperature as a function of the governing parameters: ratios of nanofluid to water and porous media to water thermal conductivities, nanoparticles volume fraction, and Rayleigh number. The applicability of the correlation was illustrated for a practical application case. It was found that, for some cases, the proposed thermal control system improves power dissipation by a factor of 33% as compared with the case of pure water (2 kW versus 1.5 kW).

* Corresponding author.
E-mail address: emortega@uvigo.es (E. Martin).

https://doi.org/10.1016/j.csite.2022.101869
Received 10 December 2021; Received in revised form 9 February 2022; Accepted 12 February 2022
Available online 15 February 2022

Nomenclature

a	thermal diffusivity (m^2s^{-1})
C	specific heat at constant pressure ($J.kg^{-1}K^{-1}$)
g	gravity acceleration ($m.s^{-2}$)
H	height of the cylinder (m)
I	current intensity (A)
$k(\varphi)$	function in eq. (11.a), defined in eq. (11.b)
L	distance $L = R_e - R_i$ (m)
$m(\lambda^*)$	function in eq. (11.a), defined in eq. (11.c)
P	power (W)
q	generated heat flux (Wm^{-2})
Q	measured global heat flux (Wm^{-2})
R_e	radius of the cavity (m)
R_i	radius of the active cylinder (m)
Ra_L	Rayleigh number (−)
S	Contact surface with nanofluid saturated porous medium (m^2)
S_i	surface of the *i*th element (m^2)
S_h	lateral surface of the antenna (m^2)
T	temperature (K)
T_c	average temperature of the cavity (K)
$\overline{T}_h$	average temperature of the antenna (K)
T_i	temperature of the *i*th element (K)
U	voltage (V)

Greek symbols

β	volumetric expansion coefficient (K^{-1})
δ	difference $\delta = \overline{\Delta T}_c - \overline{\Delta T}_m$ (K)
ΔY	absolute uncertainty for a given parameter Y (unit of Y)
$\Delta Y/Y$	relative uncertainty for a given parameter Y (%)
$\overline{\Delta T}$	difference temperature $\overline{\Delta T} = \overline{T}_h - T_c$ (K)
ε	porosity
φ	Nanoparticles volume fraction (%) in nanofluid
λ	thermal conductivity ($Wm^{-1}K^{-1}$)
λ^*	dimensionless thermal conductivity (−)
μ	dynamic viscosity (Pa.s)
ρ	density ($kg.m^{-3}$)

Subscripts

Cu	solid Copper nanoparticles
ca	calculated
m	measured
nf	nanofluid
sp	solid matrix of the porous medium
spm	saturated porous medium
w	base fluid (pure water)

1. Introduction

The use of home automation, that applies to both individual apartments and groups of buildings, is becoming the tendency in the field of modern housing development. When conjoint installations are planned, often preferred because they reduce operating and maintenance costs, a collective antenna is normally used. Its purpose is to manage equipment in real and delayed time, both on site and remotely, and to serve for big data transmission in connection to building maintenance and safety as described by Martin-Garin et al. [1]. From a thermal viewpoint, these antennae are characterized by the strong heat flux generated by their internal electronic assembly that may lead to temperatures so high that they could even cause malfunctions and shut down. Therefore, their thermoregulation is critical for a reliable system operation.

Normally, air natural convection is preferred in these types of thermal control systems given its well-known advantages; among

others: simplicity of design and robustness of operation. This was the case in the study by Kim et al. [2] where the convective heat transfer coefficient was determined for a vertical surface equipped with micro-fin arrays. However, air thermophysical properties, notwithstanding their well proven applicability in engineering applications, are sometimes insufficient when a large volumetric heat flux is generated, as in the case discussed here. In this situation, other working fluids could be used such as water, oils, or alcohols with different compositions and thermophysical properties (Bharti et al. [3], Baïri [4]). In this context, nanofluids have recently proven to be highly effective in enhancing heat transfer, as shown, for instance, in the experimental work of Xu et al. [5] dealing with opto-electronic devices. Furthermore, the improvement of nanofluid's manufacturing techniques, their ease of use, and the reduction in their cost price makes them more and more attractive (Ali [6] and Sabour et al. [7]). Also, their association with porous materials leads to further enhanced heat transfer as highlighted in several works dealing with components and cavities of different shapes and various nanofluids: Abu-Nada and Oztop [8], Sheikholeslami et al. [9], Baïri and Laraqi [10], Sheremet et al. [11], Alilat [12], Pourfazad et al. [13], Hajipour et al. [14], Sharaf et al. [15], Alilat et al. [16], Salehi et al. [17], Gholinia et al. [18], El-Shorbagi et al. [19] and Li et al. [20].

The thermophysical characteristics of the nanofluid play an important role in the heat exchange phenomena, as shown in Toghraie et al. [21], Soltani et al. [22], Baïri [23] and in the recent critical review published by Zahmatkesh et al. [24]. This review describes, among others, the effect of nanoparticle shape, volume fraction, and temperature on the constitutive characteristics of the nanofluid, whose effective thermal conductivity and dynamic viscosity are the key thermophysical properties for any modelling approach. In this context, several global models have been described in the specialized literature, but it should be noted that they show a large dispersion. Accordingly, research is intensifying to classify those that present the best results validated by measurements, and to associate them with precise operating conditions.

Basic models tend to follow, as a reference, the formulation proposed by Maxwell [25] and Brinkman [26] (spherical nanoparticles), and Hamilton and Crosser [27] (non-spherical), to determine the effective thermal conductivity and dynamic viscosity of the nanofluid. A practical implementation of the Hamilton–Crosser model [27] could be found in the work by Abu-Nada et al. [28]. Another relevant model is the one proposed by Koo and Kleinstreuer [29] that decomposes the effective thermal conductivity into a static part (Maxwell) and another part taking accounting for the contribution of Brownian motion. Recent applications of this model could be found in the works of Sharafeldin et al. [30], and Babajani et al. [31]. An interesting conclusion of another model, this time proposed by Timofeeva et al. [32], was that the Brownian motion has less influence on the effective viscosity than on the effective thermal conductivity. A relevant study, that complements those reviewed so far, is the one published by Corcione [33] in which the proposed constitutive correlations are of an empirical nature. The study showed that the actual nanofluid effective thermal conductivity tends to be either under or over-estimated by Maxwell's model [25], and the effective viscosity to be under-estimated by the Brinkman model [26].

The present work deals with the thermal control of a cylindrical antenna placed vertically. The envisaged application is for its use in collective integrated home automation. The antenna is contained in a concentric quasi-cylindrical isothermal enclosure. Cooling is provided by a porous matrix saturated with H_2O–Cu nanofluid whose nanoparticles volume fraction varies in the range from 0 (pure water) to 5%. The ratio between thermal conductivity of the porous matrix to that of water spans from 4 to 41.2. A new correlation is developed that allows for determination of the mean temperature of the antenna as a function of the governing parameters. The results obtained could be used to optimize the global design of the antenna to favor its actual implementation.

2. Description of the problem

The problem consisted of the determination of the average temperature, $\overline{T}_h$, of a cylindrical, vertical, finned antenna during steady state operation. A constant heat flux q was generated on the inside of the antenna whose lateral wall contained eight rectangular fins

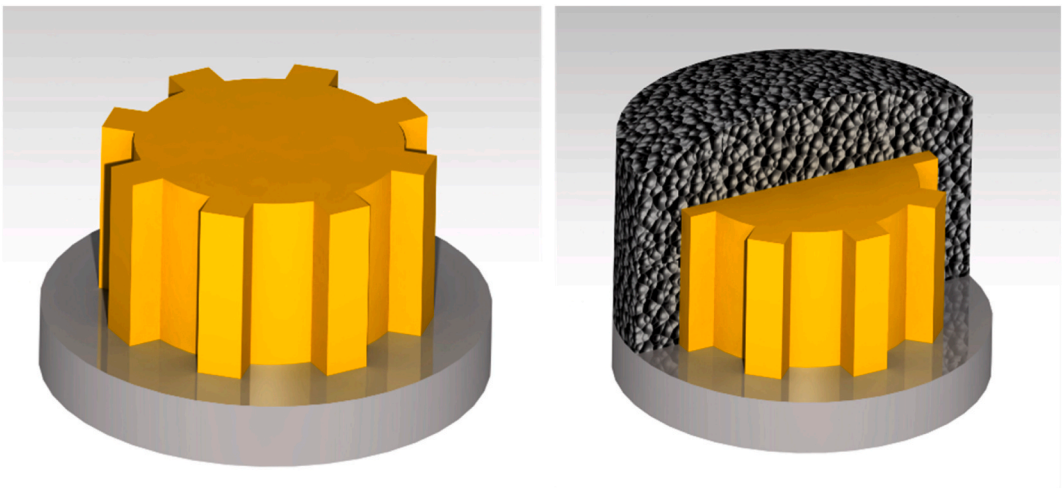

Fig. 1(a). 3D sketch of the considered configuration.

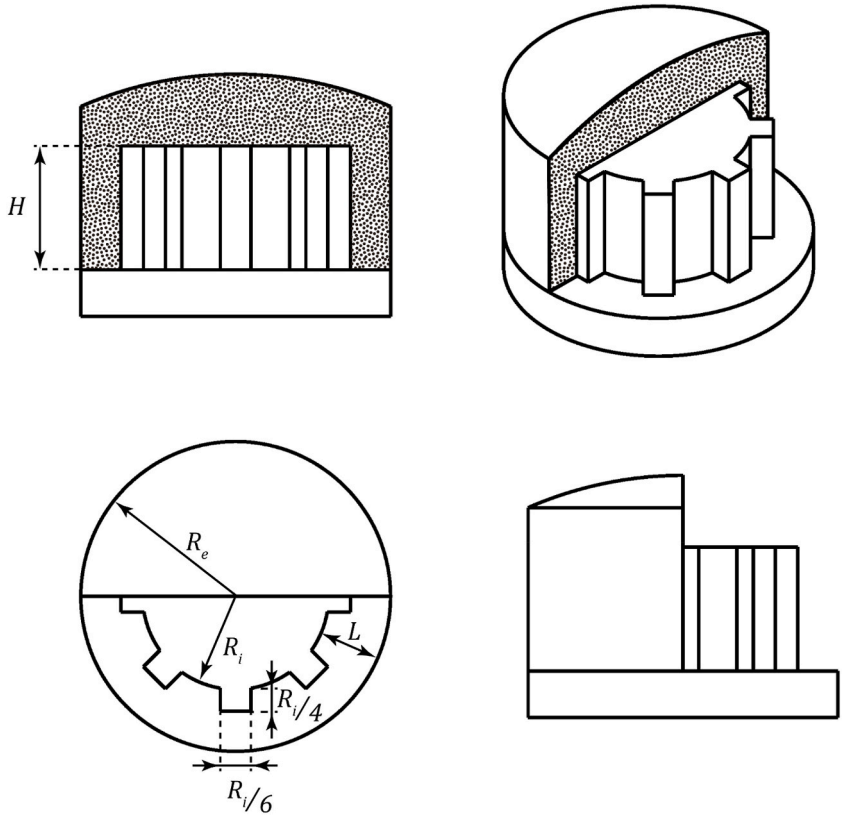

Fig. 1(b). 2D views of the considered configuration.

arranged in the vertical direction. This setup was enclosed in a quasi-cylindrical cavity filled with a porous matrix saturated with a Water-Copper based nanofluid. The enclosing cavity had a double outer wall that was kept isothermal at temperature T_c by means of a water-glycol dilution forced to flow in between the double wall. Two sketches (3D and 2D) of the considered configuration are presented in Fig. 1(a) and Fig. 1(b), respectively.

R_i, R_e, H, and S_h denote inner and external radius of the system, height, and lateral surface area respectively. The difference $(R_e - R_i)$ was denoted as L. The horizontal base of the enclosure (cavity plus antenna) was insulated and could be considered nearly adiabatic. The nanoparticles volume fraction in the Water-Copper nanofluid was varied between 0 (pure water) up to 5%. The properties (thermal conductivity, λ, density, ρ, specific heat, C, thermal expansion coefficient, β, and dynamic viscosity, μ) of both water and copper nanoparticles (when applicable) are detailed in Table 1, see Abu-Nada et al. [28] and Rashidi et al. [34]. The ratio between the thermal conductivity of the porous matrix (porosity $\varepsilon = 0.97$) and the water was varied in the range from 4.0 up to 41.2.

2.1. Nanofluid properties

The Water-Copper nanofluid used in the experiments was regularly replaced to avoid problems like agglomeration and sedimentation. Regarding the determination of its thermophysical properties, the Maxwell [25] and Brinkman [26] models were used. The experimental applicability of these models has been tested by Baïri [35] and Baïri et al. [36]. The effective thermal conductivity, λ_{nf}, dynamic viscosity, μ_{nf}, density, ρ_{nf}, thermal expansion coefficient, β_{nf}, and specific heat, C_{nf}, of the nanofluid (subscript nf) were defined as follows:

Table 1
Thermophysical characteristics of pure water and Copper nanoparticles.

	Pure water (w)	Copper nanoparticles (Cu)
λ (W m^{-1} K^{-1})	0.613	401
ρ (kg m^{-3})	997	8933
C (J kg^{-1} K^{-1})	4180	395
β (K^{-1})	2.1×10^{-4}	1.67×10^{-5}
μ (Pa s)	8.91×10^{-4}	

$$\lambda_{nf} = \left(\frac{\lambda_{Cu} + 2\lambda_w - 2\varphi(\lambda_w - \lambda_{Cu})}{\lambda_{Cu} + 2\lambda_w + \varphi(\lambda_w - \lambda_{Cu})}\right)\lambda_w \tag{1}$$

$$\mu_{nf} = \frac{\mu_w}{(1-\varphi)^{2.5}} \tag{2}$$

$$\rho_{nf} = (1-\varphi)\rho_w + \varphi\rho_{Cu} \tag{3}$$

$$\beta_{nf} = \frac{(1-\varphi)(\rho\beta)_w + \varphi(\rho\beta)_{Cu}}{\rho_{nf}} \tag{4}$$

$$C_{nf} = \frac{(1-\varphi)(\rho C)_w + \varphi(\rho C)_{Cu}}{\rho_{nf}} \tag{5}$$

where φ is the volume fraction of the nanofluid. Properties of the nanofluid saturated porous media (subscript *spm*) were calculated using the porosity ε.

$$\lambda_{spm} = \varepsilon\lambda_{nf} + (1-\varepsilon)\lambda_{sp} \tag{6}$$

$$(\rho C)_{spm} = \varepsilon(\rho C)_{nf} + (1-\varepsilon)(\rho C)_{sp} \tag{7}$$

The ratio between thermal conductivity of the porous media's solid matrix (subscript *sp*) and that of water, λ^*, was a governing parameter too.

$$\lambda^* = \frac{\lambda_{sp}}{\lambda_w} \tag{8}$$

2.2. Description of the experimental setup

The main subsystems (see the sketch presented in Fig. 2(a)) of the experimental rig were:

- The thermoregulated bath that generated a glycol-water flow at the desired temperature, T_c, in the range between 278 and 300 K (±0.1 K).
- The calibrating thermometer needed to calibrate all the thermocouples of the assembly.
- The data acquisition unit that collected the thermal and electrical data of the tested assembly.
- The stabilized power supply enabling the antenna to be powered on. Current intensity I and voltage U were measured with integrated high precision multimeters (2×10^7 points, 6 digits). Their absolute uncertainties were $\Delta I = \pm 0.1$mA and $\Delta U = \pm 0.01$ V. Relative uncertainty of the resulting global power $P = UI$ was determined by means of the well-known partial derivative method as $\Delta P/P = \Delta U/U + \Delta I/I$. The uncertainty of the corresponding global measured heat flux $Q = P/S_h$ was, then, calculated by means of the same derivative method $\Delta Q/Q = \Delta P/P + \Delta S_h/S_h$. After accounting for the measurement uncertainties of the antenna's dimensions, calculations lead to $\Delta Q/Q$ varying in the span from 0.8 to 1.7%.
- The computer needed to collect and process the measured physical parameters.

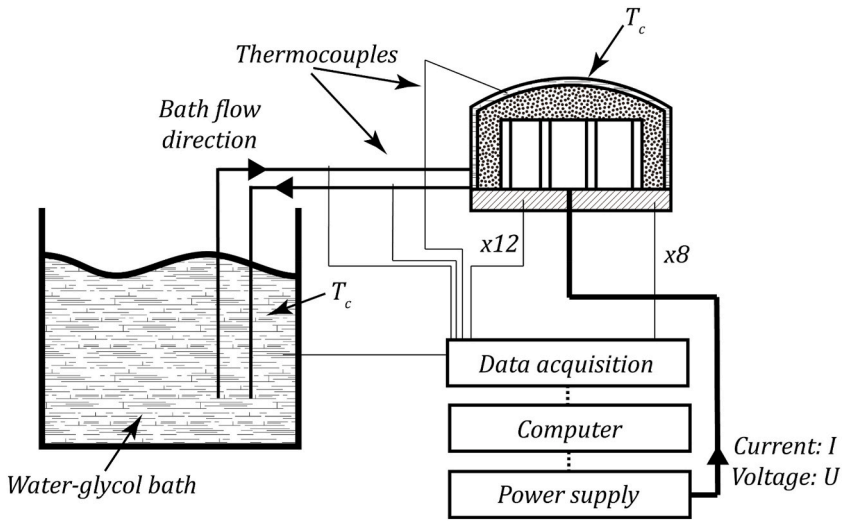

Fig. 2(a). Sketch of the experimental rig.

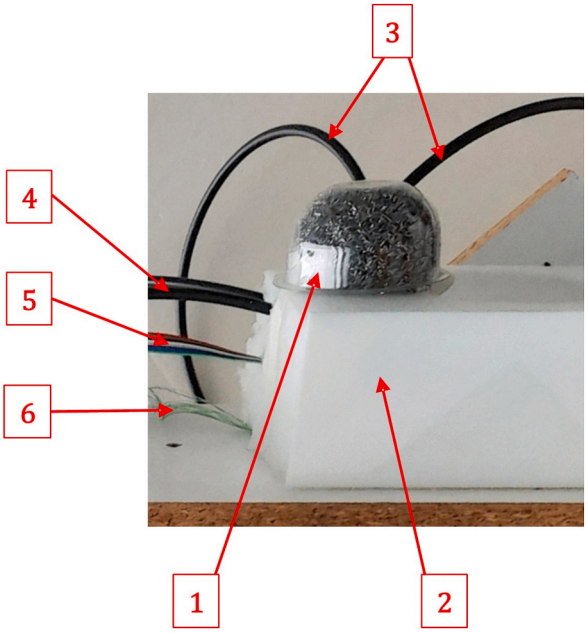

Fig. 2(b). Photograph of the tested assembly.

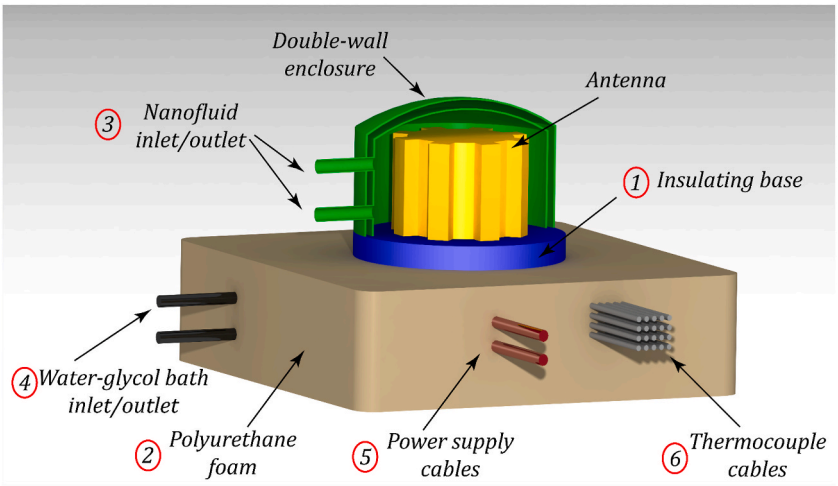

Fig. 2(c). Sketch of the tested assembly.

Regarding the tested assembly, see Fig. 2(b) and Fig. 2(c), the antenna was installed on a circular base of insulating material (number 1 in Fig. 2(b)) placed on top of a thick extruded polyurethane foam plate (number 2 in Fig. 2(b)). The average thermal conductivity of this insulating material in the operating temperature range (5–70 °C) was 0.036 ± 0.002 $Wm^{-1}K^{-1}$ measured by using the Transient Plane Source (TPS) method [37,38]. The thermal conductivity of the porous material, λ_{sp}, was also measured by means of the same TPS method. Two materials were tested in the experimental campaign with $\lambda^* = \lambda_{sp}/\lambda_w = 4.8$ and 38.4 (± 0.3) respectively. In addition, the case without porous material ($\lambda^* = 0$) was also tested.

The porous medium consisted of shavings of these materials made with a lathe. Their high porosity $\varepsilon = 0.97 \pm 0.02$ was measured by using the Mercury Intrusion Porosimetry Method (IPM) [39]. The Water-Copper nanofluid was introduced into the cavity by means of two pipes (number 3 of Fig. 2(b) and (c)). The purpose of these inlet/outlet pipes was just to fill and empty the cavity before and after the experiments respectively but were closed during the experimental campaigns. Two different concentrations of Copper nanoparticles were considered in the tests. The corresponding volume fractions were $\varphi = 1.33$ % and 4.81 % (± 0.02). In addition, tests were also performed with pure water ($\varphi = 0\%$). Thermal conductivity of these three fluids (two Water-Copper nanofluids plus pure water) was measured with the TPS method. The water-glycol mixture generated by the thermostatic bath flowed into the double thickness outer wall of the cavity through the tubes indicated with number 4 in Fig. 2(b) and (c). This flow kept the enclosure's wall at

the desired cold temperature T_c within ±0.1 K.

The antenna was powered by the wiring (5) connected to the stabilized power supply. Thermocouple cables (number 6) were connected to the data acquisition unit. Thermal conditions of the system were measured by means of 0.05 mm diameter K-type thermocouples calibrated at ± 0.1 K by means of the calibrating thermometer. Measurements were performed at intervals of 0.05 s until the steady state was reached. This steady state was assumed to be hold when the temperature variation was less than 0.5%. The cold temperature T_c was measured at both the inlet and outlet lines of the refrigerant fluid, as well as at another station on the internal surface of the cavity. Their values differed by less than 0.2 K when the fluid flow was adjusted correctly.

The surface temperature of the antenna was measured at twelve points evenly distributed on the cylinder's lateral area. The temperature $\overline{T}_h$ considered in this experimental approach was the arithmetic average of the measured surface temperatures. The temperature of the cavity's base was measured at 4 points distributed uniformly on the internal surface of the base and at other 4 points located on its opposite surface (the external face). This allowed for the determination (using the linearized Fourier law) of the

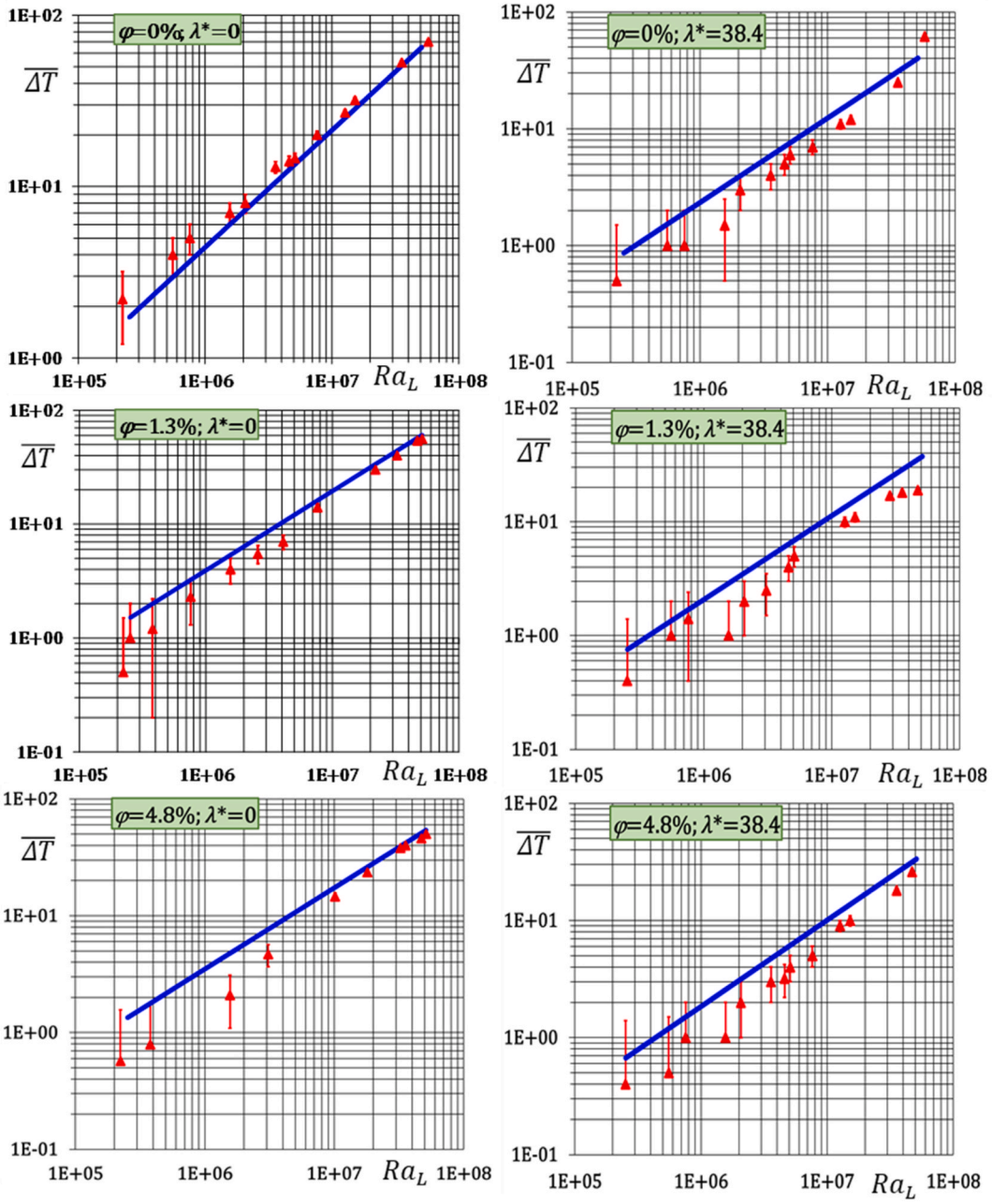

Fig. 3. Evolution of $\overline{\Delta T} = \overline{T}_h - T_c$ versus Ra_L for some (λ^*, φ) combinations.

conduction heat transfer passing through the insulating plate. Tests based on the most unfavourable configuration (the one with the highest measured heat flux Q) showed that the conductive losses associated to the insulating plate were very low, of about $0.02Q$. Since the radiative heat flux is zero in this experimental setup, the heat flux generated by the antenna q was considered to be $0.98Q$, measured with a relative uncertainty of $\Delta q/q = 2.5\%$.

The Rayleigh number was defined as:

$$Ra_L = \left(\frac{\beta\rho}{\mu\lambda a}\right)_w gL^4 q \tag{9}$$

where a is the thermal diffusivity. With this definition, the relative uncertainty of the Rayleigh number was determined using a maximum relative uncertainty of 0.5% for all thermophysical characteristics of the base fluid (water) and for the distance L . The

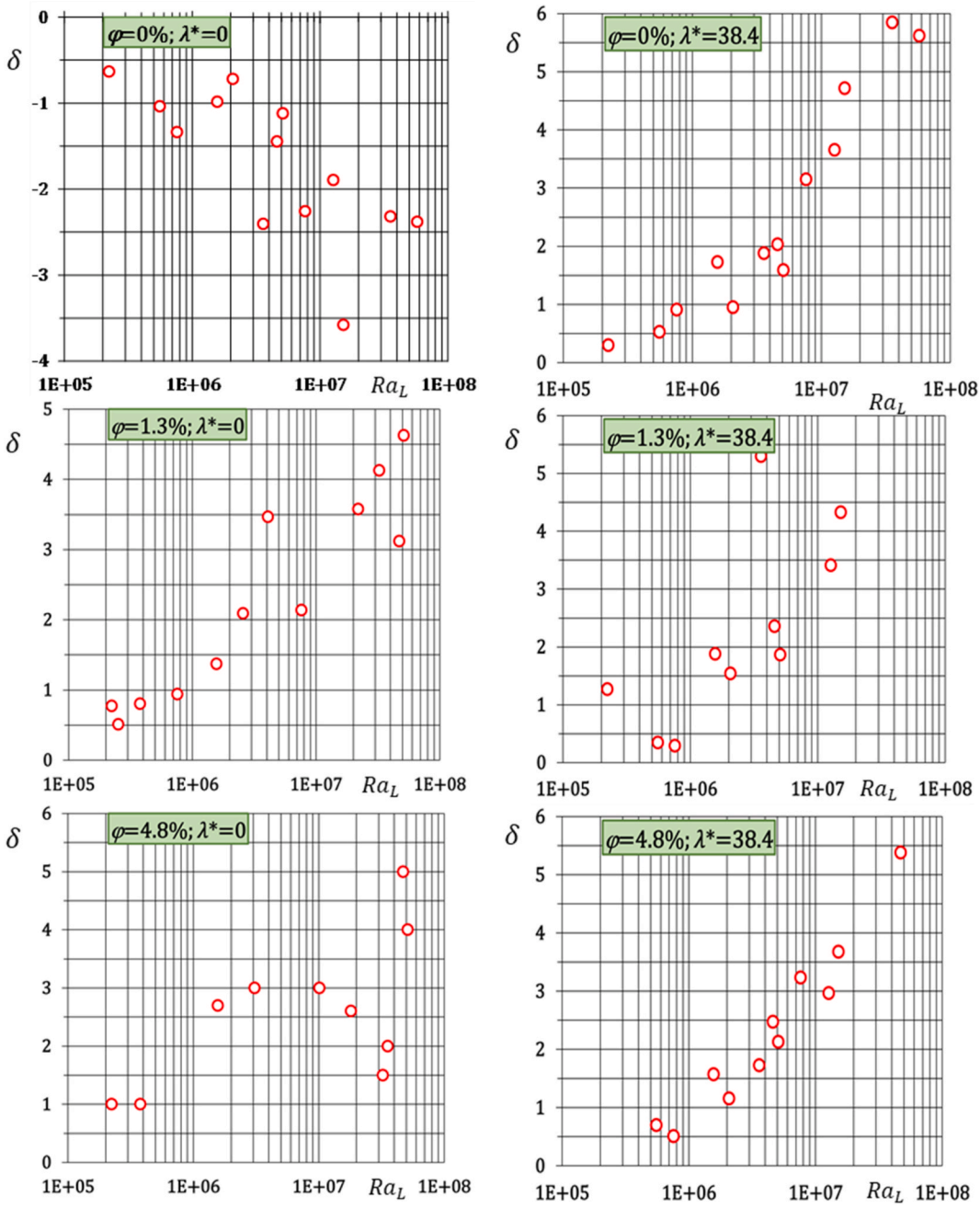

Fig. 4. Evolution of the difference $\delta = \overline{\Delta T}_{ca} - \overline{\Delta T}_m$ versus Ra_L for some (λ^*, φ) combinations.

maximum value that was obtained was $\Delta Ra/Ra \sim 7\%$. Several values of the Rayleigh number were tested in the range from $3.43\text{x}10^5$ up to $5.08\text{x}10^7$ (covering about two orders of magnitude).

3. Numerical approach

The numerical approach of the considered problem is based on the governing equations presented in several documents such as the work by Patankar [40] and Bejan [41]. The computation procedure adopted here is the same as that of the recent study by Martin et al. [42] dealing with the numerical simulation of a similar problem, where the reader could consult the details of the algorithm. Then, to lighten this manuscript, only the elements necessary for its understanding are presented here.

The computational domain was discretized with 553,523 elements of various shapes with a refinement on the lateral surface of the antenna. This operation allowed for the precise determination of the thermal gradients field at the interface of the antenna, and the corresponding local temperatures. Solution of the governing system was obtained by means of a home-made software based on the control volume method associated with the SIMPLE algorithm. The entire computational domain, including the antenna, was initially assumed to be at the lower T_c temperature. During the numerical convergence process, the thermal gradient was set to zero at the horizontal base of the configuration, while the external cavity was maintained at isothermal temperature T_c. A constant heat flux q was generated by the antenna, and the no-slip condition was imposed on the external face of the antenna and internal face of the enclosure. The average temperature of the antenna $\overline{T}_h$ was obtained by weighting the local elements temperatures T_i with the corresponding surfaces S_i:

$$\overline{T}_h = \frac{1}{S_h}\oint T_i dS_i \tag{10}$$

These calculations were carried out with the nanofluid properties obtained after the Maxwell and Brinkman models, Eq. (1)–(5).

4. Experimental results and comparison between the two approaches: experimental and numerical

Results of the $\overline{\Delta T} = \overline{T}_h - T_c$ measurements versus Ra_L accompanied by their uncertainty are presented in Fig. 3 for some representative (λ^*, φ) combinations. The Ra_L uncertainties are, intentionally, not represented given the chosen logarithmic scale.

The next step was, first, to compute a number of cases in the space of parameters, and, second, to compare the results obtained to those obtained experimentally. This comparison was performed in terms of the parameter $\delta = \overline{\Delta T}_{ca} - \overline{\Delta T}_m$, where $\overline{\Delta T}_{ca}$ is the calculated $\overline{\Delta T}$, and $\overline{\Delta T}_m$ is the measured $\overline{\Delta T}$. The results obtained are presented in Fig. 4. In the case of cooling with pure water and without porous material ($\lambda^* = 0,\ \varphi = 0$), the measured values $\overline{\Delta T}_m$ are almost systematically greater than the calculated ones $\overline{\Delta T}_{ca}$, with a difference varying between 0.5 and 3.5 K. However, the measurements are lower for all the configurations affected by the nanofluid ($\varphi \neq 0$). The measurement-calculation deviations vary between 1 and 5.5 K. The highest are observed for the highest concentrations of nanoparticles ($\varphi = 4.81\%$), for all the values of the λ^* ratio. These results are acceptable and provide and additional validation of the numerical model.

The practical outcome of all these results is the generation of a correlation for $\overline{\Delta T}$ as function of the four governing parameters of the problem; namely: λ_w/λ_{nf}, φ, λ^*, and Ra_L. The correlation is as follows:

$$\overline{\Delta T} = 3.532\text{x}10^{-4}\left(\frac{\lambda_w}{\lambda_{nf}}\right)[k(\varphi)m(\lambda^*)]^{-1}Ra_L^{0.683} \tag{11.a}$$

where:

$$k(\varphi) = \begin{cases} 1\ for\ \varphi = 0\ (\text{pure water}) \\ \\ 1.45\varphi^{0.03}Ra_L^{-0.012}\ for\ 1\% \le \varphi \le 5\% \end{cases} \tag{11.b}$$

$$m(\lambda^*) = \begin{cases} 1\ for\ \lambda^* = 0 \\ \\ 10.3(\lambda^*)^{-0.31}Ra_L^{-1+0.86(\lambda^*)^{0.03}}\ for\ 4 \le \lambda^* \le 41.2 \end{cases} \tag{11.c}$$

$$\frac{\lambda_w}{\lambda_{nf}} = \frac{\lambda_{Cu} + 2\lambda_w + \varphi(\lambda_w - \lambda_{Cu})}{\lambda_{Cu} + 2\lambda_w - 2\varphi(\lambda_w - \lambda_{Cu})} \tag{11.d}$$

Correlation (11.a) for $\overline{\Delta T}$ exhibits dependence on four parameters: λ_w/λ_{nf}, φ, λ^*, andRa_L. The first two parameters, $\lambda_w/\ \lambda_{nf}$ and φ, are linked via relations (11.b) and (11.d). Assuming that the term $Ra_L^{-0.012}$ adds up to the $Ra_L^{0.683}$ term in correlation (11.a), changing φ from 0 to 0.01 and to 0.05 decreases $\overline{\Delta T}$ by a factor of 23% and 35% respectively. On the other hand, modifying λ^* from 0 to 4 and to 41.2 decreases $\overline{\Delta T}$ by a factor of 20% and 40% respectively (for a typical Ra_L of 10^7). This suggests that, from the physics point of view, the influence of the base fluid (nanofluid or not), and the presence (or not) of the porous matrix have a similar influence on the efficiency of the proposed thermal control system. In a sense, this could be expected because the presence of both effects has the practical outcome

of increasing the effective thermal conductivity of the medium inserted in between the heat source (the antenna) and the external enclosure. The main finding has been that, in the present configuration, both effects play a role whose influence is of the same order of magnitude.

4.1. Practical application case

As an example of application of the correlations that were developed, a collective communications antenna was considered. Dimensions of this case where $R_i = 0.025$ m, with $L = 0.025$ m, and $H = 0.15$ m. The antenna had 8 fins such as the ones shown in Fig. 1, providing a contact surface with the nanofluid saturated porous medium of $S = 0.041$ m^2. The same two porous media considered in the experiment where implemented here, being their thermal conductivities λ_{sp} equal to 2.33 and 25.3 W/mK, respectively (λ^* equal to 3.8 and 41.2). The nanofluid was, also, the same. A concentric quasi-cylindrical enclosure (thermoregulated with a bath of glycol-water) at three different temperatures T_c, equal to 5, 10 and 20 °C, was taken as the external boundary condition.

Nanoparticles concentrations were considered in the range from $\varphi = 1\%$ to $\varphi = 5\%$. The limit case of pure water ($\varphi = 0\%$) was accounted for as well. The temperature correlation (11.a), that is linked with the Nusselt correlation proposed in Ref. [42], was used to evaluate the heat transfer in the saturated porous media. A prescribed maximum temperature $\overline{T}_h = 60°C$ at the antenna surface was imposed, which ensures safe thermal gradients for the electronic components inside the antenna.

The heat transfer taking place between the antenna and the saturated porous media was solved iteratively to obtain the unknown dissipated power P. Rayleigh numbers where in the range from $3.43\ 10^5$ up to $3.66\ 10^6$. The results obtained are shown in Fig. 5 for the different thermal conductivities λ_{sp} and enclosure temperatures T_c considered. The dissipated power P for the most favorable case, $\lambda_{sp} = 25.3$ W/mK and $\varphi = 5\%$, was approximately equal to 2 kW, while for the worst-case scenario, $\lambda_{sp} = 2.33$ W/mK and $\varphi = 0\%$, P was equal to 0.2 kW (one order of magnitude lower).

In the most favorable conditions: $T_c = 5\ °C$, $\lambda_{sp} = 41.2\ \lambda_w$, $\varphi = 5\%$, implementation of the proposed thermal control system allows for an improvement of dissipated power of the order of 33% as compared with the case of pure water (2 kW versus 1.5 kW). In the less favorable case, $T_c = 20\ °C$, $\lambda_{sp} = 3.8\ \lambda_w$, $\varphi = 1\%$, the system presents marginal gains, only, as compared to the case of pure water. If an antenna with the same dimensions equipped with a conventional approach to heat transfer is considered (free convection to the ambient air from the cylindrical cover enclosing the electronics), the dissipated heat would be of the order of 0.01 kW. This means that, in the most favorable case, the proposed system outperforms conventional approaches by a factor of 200 (2 kW versus 0.01 kW). This, of course, comes at the expense of a more complex architecture that requires the preparation of the nanofluid, the fitting of the porous media, and the implementation and operation of the low temperature water-glycol circuit, among others. In a sense, this directs the proposed system towards applications in which power density is very high, and cost may not be a problem.

5. Conclusions

The average surface temperature of a finned cylindrical antenna used for controlling collective home equipment was determined in this experimental study. Due to the large heat flux per unit area that this type of antenna (and application) generates, novel thermal control approaches that met requirements are demanded, being this a non-stop trend due to the continuous growth (in complexity and demand) of electronic systems. For this case, porous materials saturated with water-based Copper nanofluid were experimentally tested for its thermal regulation.

A number of configurations were considered in the study. They were obtained by varying the nanofluid's volume fraction between 0 (pure water) and 5%, and the ratio between the conductivity of the porous material and that of the water in the span from 4 to 41.2. The study has shown that appropriate selection of the Rayleigh number, nanofluid's volume fraction, and thermal conductivity of the porous matrix allows a temperature (for an average surface antenna) compatible with its operating conditions requirements. The experimental results obtained have been compared, for consistency reasons, with a numerical simulation method developed, also, by the authors. Differences between the experiment and the numerical simulations were found to be small and, generally, fell inside the uncertainty band of the experiments. To facilitate the use of the proposed thermal control approach in engineering applications, the experimental results were generalized in the form of a correlation that depends of the governing problem parameters.

To get a better insight into the actual engineering design aspects of the proposed approach, a practical application case was considered. The main conclusions of this practical application case were twofold. First, it was found that performance of the thermal control system is very sensitive to changes in the governing parameters. For instance, in the most favorable conditions: $T_c = 5\ °C$, $\lambda_{sp} = 41.2\ \lambda_w$, $\varphi = 5\%$, the system presented an improvement of dissipated power of the order of 33% (2 kW versus 1.5 kW) as compared with the case of using pure-water only within the same solid porous material. In the less favorable case, $T_c = 20\ °C$, $\lambda_{sp} = 3.8\ \lambda_w$, $\varphi = 1\%$, the system presented only marginal gains when compared to the case of pure water. This means that to get the maximum benefit, the system operation parameters need to be tuned carefully, and this why the availability of a practical engineering correlation facilitates this tuning. Second, it was found that this thermal control system outperforms by a very large factor (of the order of 100) that of conventional systems based of natural convection. The drawback is that the simplicity and robustness of the conventional approach is offset by the larger technical and operational complexity of the proposed approach. Talking in practical engineering terms, this means that the target niche of this proposed approach are those advanced electronic systems (an antenna in this case) characterized by very large values of heat flux per unit area.

Regarding the physical aspects of the problem, one of the main findings of the study is that the base fluid (either nanofluid or not) and the presence (or not) of the porous matrix exert an influence on the system thermal control that is of the same order of magnitude. This, for practical engineering design purposes, is important because it suggests that both effects need to be tuned in parallel in actual thermal control systems.

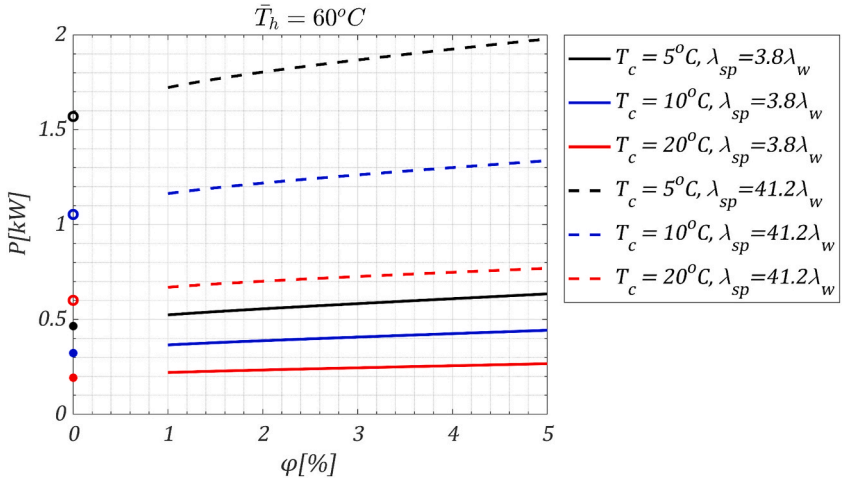

Fig. 5. Dissipated power for the application case under different conditions.

Acknowledgements

Partial funding for open access charge: Universidade de Vigo/CISUG.

Declaration of competing interest

The authors declare that they have no known competing financial interests or personal relationships that could have appeared to influence the work reported in this paper.

References

[1] A. Martín-Garín, J.A. Millán-García, A. Baïri, J. Millán-Medel, J.M. Sala-Lizarraga, Environmental monitoring system based on an open source platform and the internet of things for a building energy retrofit, Autom. ConStruct. 87 (2018) 201–214.
[2] J.S. Kim, B.K. Park, J.S. Lee, Natural convection heat transfer around microfin arrays, Exp. Heat Tran. 21 (1) (2008) 55–72.
[3] O.S. Bharti, A.K. Saha, M.K. Das, S. Bansal, Simultaneous measurement of velocity and temperature fields during natural convection in a water-filled cubical cavity, Exp. Therm. Fluid Sci. 99 (2018) 272–286.
[4] A. Baïri, Transient thermal characteristics of airborne electronic equipment with discrete hot bands in square cavities, Appl. Energy 85 (10) (2008) 951–967.
[5] H. Xu, C. Chang, J. Zhang, J. Xu, H. Chen, H. Guo, B. Fu, C. Song, W. Shang, P. Tao, T. Deng, Transparent nanofluids with high thermal conductivity for improved convective thermal management of optoelectronic devices, Exp. Heat Tran. 35 (2) (2022) 183–195.
[6] H.M. Ali, Hybrid Nanofluids for Convection Heat Transfer, Academic Press, 2020.
[7] M. Sabour, M. Ghalambaz, A. Chamkha, Natural convection of nanofluids in a cavity: criteria for enhancement of nanofluids, Int. J. Numer. Methods Heat Fluid Flow 27 (7) (2017) 1504–1534.
[8] E. Abu-Nada, H.F. Oztop, Effects of inclination angle on natural convection in enclosures filled with Cu–water nanofluid, Int. J. Heat Fluid Flow 30 (2009) 669–678.
[9] M. Sheikholeslami, M.B. Gerdroodbary, R. Moradi, A. Shafee, Z. Li, Numerical mesoscopic method for transportation of H2O-based nanofluid through a porous channel considering Lorentz forces, Int. J. Mod. Phys. C 30 (2n03) (2019), 1950007.
[10] A. Baïri, N. Laraqi, Experimental quantification of natural convective heat transfer within annulus space filled with a H_2O-Cu nanofluid saturated porous medium. Application to electronics cooling, Exp. Heat Tran. 32 (4) (2019) 364–375.
[11] M. Sheremet, I. Pop, H.F. Öztop, N. Abu-Hamdeh, Natural convection of nanofluid inside a wavy cavity with a non-uniform heating, Int. J. Heat Fluid Flow 27 (4) (2017) 958–980.
[12] N. Alilat, Natural convective heat transfer in the air-filled interstice between inclined concentric hemispheres, Int. J. Heat Fluid Flow 27 (10) (2017) 2375–2384.
[13] E. Pourfazad, K. Ghadiri, A. Behrangzade, M. Ashjaee, Experimental investigation of heat transfer and pressured drop of alumina-water nano-fluid in a porous miniature heat sink, Exp. Heat Tran. 31 (6) (2018) 495–512.
[14] M. Hajipour, A. Molaei Dehkordi, Analysis of nanofluid heat transfer in parallel-plate vertcal channels partially filled with continuous porous medium, Int. J. Therm. Sci. 55 (2012) 103–113.
[15] O.Z. Sharaf, R.A. Taylor, E. Abu-Nada, On the colloidal and chemical stability of solar nanofluids: from nanoscale interactions to recent advances, Phys. Rep. 867 (2020) 1–84.
[16] N. Alilat, O. Haddad, A. Baïri, Numerical study of natural convection of ZnO-water nanofluid enclosed between two inclined and concentric hemispheres, Eur. Phys. J. Plus 135 (2) (2020) 146.
[17] S. Salehi, A. Nori, Kh Hosseinzadeh, D.D. Ganji, Hydrothermal analysis of MHD squeezing mixture fluid suspended by hybrid nanoparticles between two parallel plates, Case Stud. Therm. Eng. 21 (2020), 100650.
[18] M. Gholinia, Kh Hosseinzadeh, D.D. Ganji, Investigation of different base fluids suspend by CNTs hybrid nanoparticle over a vertical circular cylinder with sinusoidal radius, Case Stud. Therm. Eng. 21 (2020), 100666.
[19] M.A. El-Shorbagy, F. Eslami, M. Ibrahim, P. Barnoon, W.F. Xia, D. Toghraie, Numerical investigation of mixed convection of nanofluid flow in a trapezoidal channel with different aspect ratios in the presence of porous medium, Case Stud. Therm. Eng. 25 (2021), 100977.
[20] Z. Li, P. Barnoon, D. Toghraie, R.B. Dehkordi, M. Afrand, Mixed convection of non-Newtonian nanofluid in an H-shaped cavity with cooler and heater cylinders filled by a porous material: two phase approach, Adv. Powder Technol. 30 (11) (2019) 2666–2685.
[21] D. Toghraie, N. Sina, N.A. Jolfaei, M. Hajian, M. Afrand, Designing an Artificial Neural Network (ANN) to predict the viscosity of Silver/Ethylene glycol nanofluid at different temperatures and volume fraction of nanoparticles, Phys. A: Stat. Mech. Appl. 34 (1) (2019), 122142.
[22] F. Soltani, D. Toghraie, A. Karimipour, Experimental measurements of thermal conductivity of engine oil-based hybrid and mono nanofluids with tungsten oxide (WO3) and MWCNTs inclusions, Powder Technol. 371 (2) (2020) 37–44.
[23] A. Baïri, Natural convection between concentric and inclined hemispherical cavities filled with Cu-water nanofluid, J. Mol. Liq. 249 (2018) 1263–1270.

[24] I. Zahmatkesh, M. Sheremet, L. Yang, S.Z. Heris, M. Sharifpur, J.P. Meyer, M. Ghalambaz, S. Wongwises, D. Jing, O. Mahian, Effect of nanoparticle shape on the performance of thermal systems utilizing nanofluids: a critical review, J. Mol. Liq. 321 (2021), 114430.
[25] J.C.A. Maxwell, Treatise Electricity Magnetic, second ed., Clarendon Press, Oxford (UK), 1881.
[26] H.C. Brinkman, J. Chem. Phys. 20 (4) (1952) 571–581.
[27] R. Hamilton, O. Crosser, Thermal conductivity of heterogeneous two–component systems, Ind. Eng. Chem. Fundam. 1 (1962) 187–191.
[28] E. Abu-Nada, Z. Masoud, A. Hijazi, Natural convection heat transfer enhancement in horizontal concentric annuli using nanofluids, Int. Commun. Heat Mass Tran. 35 (5) (2008) 657–665.
[29] J. Koo, C. Kleinstreuer, Laminar nanofluid flow in microheat–sinks, Int. J. Heat Mass Tran. 48 (2005) 2652–2661.
[30] M.A. Sharafeldin, G. Gróf, E. Abu-Nada, O. Mahian, Evacuated tube solar collector performance using copper nanofluid: energy and environmental analysis, Appl. Therm. Eng. 162 (2019), 114205.
[31] M. Babajani, B. Ghasemi, A. Raisi, Numerical study on mixed convection cooling of solar cells with nanofluid, Alex. Eng. J. 56 (2017) 93–103.
[32] E.V. Timofeeva, J.L. Routbort, D. Singh, Particle shape effects on thermophysical properties of alumina nanofluids, J. Appl. Phys. 106 (2009), 014304.
[33] M. Corcione, Empirical correlating equations for predicting the effective conductivity and dynamic viscosity of nanofluids, Energy Convers. Manag. 25 (2011) 789–793.
[34] M.M. Rashidi, A. Hosseini, I. Pop, S. Kumar, N. Freidoonimehr, Comparative numerical study of single and two-phase models of nanofluid heat transfer in wavy channel, Appl. Math. Mech. 35 (7) (2014) 831–848.
[35] A. Baïri, Experimental study on enhancement of free convective heat transfer in a tilted hemispherical enclosure by using Water-ZnO nanofluid saturated porous materials, Appl. Therm. Eng. 148 (2019) 992–998.
[36] A. Baïri, N. Alilat, F.D. Quintana, Experimental study of free convective heat transfer through nanofluid saturated porous media around a spherical electronic component, Heat Mass Tran. 56 (11) (2020) 3085–3092.
[37] S.E. Gustafsson, Transient plane source techniques for thermal conductivity and thermal diffusivity measurements of solid materials, Rev. Sci. Instrum. 62 (1991) 797–804.
[38] TPS Hot Disk TPS 2500 manual. HOT DISK AB, (Goteborg, Sweden).
[39] Mercury Intrusion Porosimetry. https://www.mri.psu.edu/materials-characterization-lab/instruments-mcl/mercury-intrusion-porosimetry.
[40] S.V. Patankar, Numerical Heat Transfer and Fluid Flow, Series in Computational Methods in Mechanics and Thermal Science, Taylor and Francis Publishers, 1980.
[41] A. Bejan, Convection Heat Transfer, fourth ed., John Wiley & Sons, Inc., Hoboken, NJ (USA), 2013.
[42] E. Martin, F. Sastre, A. Velazquez, A. Baïri, Heat transfer enhancement around a finned vertical antenna by means of porous media saturated with Water-Copper nanofluid, Case Stud. Therm. Eng. 28 (2021), 101555.